Suborbital Measurements of Spectral Aerosol Optical Depth and Its Variability at Subsatellite Grid Scales in Support of CLAMS 2001

J. REDEMANN,[*] B. SCHMID,[*] J. A. EILERS,[+] R. KAHN,[#] R. C. LEVY,[@,##] P. B. RUSSELL,[+] J. M. LIVINGSTON,[&] P. V. HOBBS,[**] W. L. SMITH JR.,[++] AND B. N. HOLBEN[@]

[*]*Bay Area Environmental Research Institute, Sonoma, California*
[+]*NASA Ames Research Center, Moffett Field, California*
[#]*Jet Propulsion Laboratory, Pasadena, California*
[@]*NASA Goddard Space Flight Center, Greenbelt, Maryland*
[&]*SRI International, Menlo Park, California*
[**]*University of Washington, Seattle, Washington*
[++]*NASA Langley Research Center, Hampton, Virginia*

(Manuscript received 15 November 2003, in final form 5 June 2004)

ABSTRACT

As part of the Chesapeake Lighthouse and Aircraft Measurements for Satellites (CLAMS) experiment, 10 July–2 August 2001, off the central East Coast of the United States, the 14-channel NASA Ames Airborne Tracking Sunphotometer (AATS-14) was operated aboard the University of Washington's Convair 580 (CV-580) research aircraft during 10 flights (~45 flight hours). One of the main research goals in CLAMS was the validation of satellite-based retrievals of aerosol properties. The goal of this study in particular was to perform true over-ocean validations (rather than over-ocean validation with ground-based, coastal sites) at finer spatial scales and extending to longer wavelengths than those considered in previous studies. Comparisons of aerosol optical depth (AOD) between the Aerosol Robotic Network (AERONET) Cimel instrument at the Chesapeake Lighthouse and airborne measurements by AATS-14 in its vicinity showed good agreement with the largest *r*-square correlation coefficients at wavelengths of 0.38 and 0.5 μm (>0.99). Coordinated low-level flight tracks of the CV-580 during *Terra* overpass times permitted validation of over-ocean Moderate Resolution Imaging Spectroradiometer (MODIS) level 2 (MOD04_L2) multiwavelength AOD data (10 km × 10 km, nadir) in 16 cases on three separate days. While the correlation between AATS-14- and MODIS-derived AOD was weak with an *r* square of 0.55, almost 75% of all MODIS AOD measurements fell within the prelaunch estimated uncertainty range $\Delta\tau = \pm 0.03 \pm 0.05\tau$. This weak correlation may be due to the small AODs (generally less than 0.1 at 0.5 μm) encountered in these comparison cases. An analogous coordination exercise resulted in seven coincident over-ocean matchups between AATS-14 and Multiangle Imaging Spectroradiometer (MISR) measurements. The comparison between AATS-14 and the MISR standard algorithm regional mean AODs showed a stronger correlation with an *r* square of 0.94. However, MISR AODs were systematically larger than the corresponding AATS values, with an rms difference of ~0.06. AATS data collected during nine extended low-level CV-580 flight tracks were used to assess the spatial variability in AOD at horizontal scales up to 100 km. At UV and midvisible wavelengths, the largest absolute gradients in AOD were 0.1–0.2 per 50-km horizontal distance. In the near-IR, analogous gradients rarely reached 0.05. On any given day, the relative gradients in AOD were remarkably similar for all wavelengths, with maximum values of 70% $(50\ \text{km})^{-1}$ and more typical values of 25% $(50\ \text{km})^{-1}$. The implications of these unique measurements of AOD spatial variability for common validation practices of satellite data products and for comparisons to large-scale aerosol models are discussed.

1. Introduction

The Chesapeake Lighthouse and Aircraft Measurements for Satellites (CLAMS) campaign was a clear-sky, shortwave (SW) closure campaign and entailed measurements from the Chesapeake Lighthouse research platform {hereafter called COVE [the Clouds and the Earth's Radiant Energy System (CERES) Ocean Validation Experiment]}, several land sites, six research aircraft, and the *Terra* satellite (Smith et al. 2005). CLAMS research goals included validation of satellite-based retrievals of aerosol properties and vertical profiles of radiative fluxes, temperature, and water vapor. Suborbital measurements of aerosol optical depth (AOD) and columnar water vapor (CWV) were

[##] Current affiliation: Science Systems and Applications Inc., Lanham, Maryland.

Corresponding author address: Jens Redemann, BAERI/NASA Ames Research Center, MS 245-5, Moffett Field, CA 94035-1000. E-mail: jredemann@mail.arc.nasa.gov

carried out at several Aerosol Robotic Network (AERONET) sites (Holben et al. 1998) and aboard five of the six airborne platforms using a variety of techniques. The University of Washington's Convair 580 (CV-580) research aircraft carried a suite of in situ instruments to characterize aerosol properties and the ambient radiation field (Magi et al. 2005). Among the remote sensors aboard the CV-580 was the National Aeronautics and Space Administration (NASA) Ames Airborne Tracking Sunphotometer (AATS-14), which measures direct solar beam transmission through the atmosphere to determine AOD between 0.354 and 1.558 μm, as well as columnar water vapor.

Spaceborne satellite sensors offer many potential advantages for studying aerosols at regional to global scales (Kaufman et al. 2002; Ramanathan et al. 2001). Among the sensors that have provided global aerosol information in the past are the Advanced Very High Resolution Radiometer (AVHRR) and the Total Ozone Mapping Spectrometer (TOMS), even though they were not optimized for the detection of aerosols. With the launch of the Earth Observing Satellite (EOS) *Terra* in 1999, a new era of satellite-based observations of aerosols began. The Moderate Resolution Imaging Spectroradiometer (MODIS) instruments aboard *Terra* and *Aqua* (Kaufman et al. 1997) and the Multiangle Imaging Spectroradiometer (MISR) instrument (Diner et al. 1998; Martonchik et al. 1998) aboard *Terra* strive for improved radiometric calibration and are much more capable of detailed global aerosol observations. In the case of the MODIS instrument, for example, the advantages of the new sensor include its improved spectral coverage, the narrower bandwidth of the individual channels, and improved spatial resolution of 500 m (250 m for some channels, compared to 1 or 4 km for AVHRR and 50 km for TOMS). For MISR, the improved capabilities further stem from its multiangle viewing technique, which results in the ability to separate surface from atmospheric properties and provides sensitivity to particle shape. In particular, the improved spatial resolution of the new sensors allows for a better detection and identification of clouds and hence an improved separation of aerosols from clouds.

Of considerable interest to satellite-based retrievals of aerosol optical depth is small-scale (a few hundred meters or less) variability. The question arises whether an average radiance in a given scene, as measured by a satellite sensor, can be readily translated into an average AOD over the scene. For example, in preliminary validation studies of the standard MISR AOD retrieval algorithm, Kahn et al. (2001a) found that over dark water, pixel-to-pixel scene variability could contribute more to the aerosol optical depth retrieval uncertainty than uncertainties in the calibration of the MISR cameras. In the case of MODIS, spatial variability is of equally high importance. Both the MODIS over-ocean and over-land aerosol retrieval algorithms depend heavily on the spatial variability of radiances and hence also on the variability of aerosol fields in order to detect and mask cloudy pixels (Remer et al. 2005). In the case of the land algorithm, the standard MODIS cloud mask may discard pixels that contain increased AOD in the immediate vicinity ($<$500 m) of clouds. Also, the aerosol retrieval algorithm discards those pixels that have sufficient cloud contamination to place them in the upper 50% in terms of their reflectance at 0.66 μm. In the case of the ocean algorithm, cloud masking is based solely on the spatial variability of the reflectance at 0.55 μm (Martins et al. 2002). Hence, suborbital measurements of the actual spatial variability of AOD and tests of the impact of that variability on satellite radiances are crucial in assessing the adequacy of the aerosol retrieval algorithms and the cloud-screening procedures used within them.

Spatial variability on the scale of a few hundred meters can only be assessed from suborbital platforms that move fast by comparison to wind advection speeds, and only with instruments that provide data at rates of a few hertz (1 Hz being equivalent to a spatial resolution of $\sim$100 m at an aircraft speed of $\sim$200 kt or 103 m s^{-1}). Current airborne lidars are generally backscatter systems and as such deliver only limited qualitative information on aerosol variability, since the inversion of a backscatter lidar signal requires a priori knowledge of the extinction-to-backscatter (lidar) ratio (Klett 1985). When deployed on a fast-moving aircraft such as the CV-580 during CLAMS, the NASA Ames Airborne Tracking Sunphotometers (AATS-6 and AATS-14) on the other hand provide the spatial resolution, data acquisition speed, and accuracy to support the overall goals of CLAMS and other satellite validation studies. Because the AATS instruments measure the direct solar beam transmission, and are hence unaffected by surface properties, they are excellent tools for studying the spatial variability of AOD and columnar water vapor on scales of a few hundred meters. By comparison to satellite observations, however, the AATS measurements lack the advantage of an instantaneous data collection.

In this paper, we describe the AATS-14 measurements of AOD during the CLAMS experiment, with a special emphasis on assessing the spatial variability of AOD on subsatellite grid scales with a resolution ofj 100 m. We include validation measurements for the MODIS and MISR over-ocean AOD retrieval products. For MISR, the standard aerosol retrieval algorithm produces results for a grid of 16 $\times$ 16 pixels (17.6 km $\times$ 17.6 km), while the most relevant grid size for MODIS validation efforts has been 5 $\times$ 5 level 2 boxes, resulting in a grid of 50 km $\times$ 50 km at nadir. Hence, we assess AATS-14-derived AOD variability at and below these spatial scales, determining both the mean AOD at these scales as well as the maximum variability within the satellite grids. In addition, we present comparisons of AOD measurements by the airborne AATS-14 and by an AERONET Cimel sun photometer stationed at

the COVE platform (36.9°N, 75.71°W). We also analyze the AOD variability in the vicinity of the COVE site. In this way we assess the suitability of the COVE platform as a satellite validation site and support one of the overall goals of the CLAMS experiment, namely, to determine how representative measurements at the COVE site may be of the satellite grids around it.

2. Instrumentation

a. NASA Ames Airborne Tracking Sunphotometer

Similar to its predecessor AATS-6 (Matsumoto et al. 1987), AATS-14 measures direct solar beam transmission in narrow channels (with bandwidths between 2 and 5.6 nm for the wavelengths between 0.35 and 1.56 μm and 17.3 nm for the 2.1-μm channel) by using detectors in a tracking head that can rotate about two axes. Azimuth and elevation motors controlled by differential sun sensors rotate the tracking head, thereby locking onto the solar beam and keeping detectors normal to it. The instrument's tracking head mounts external to the aircraft skin, to minimize blockage by aircraft structures and also to avoid data contamination by aircraft-window effects. AATS-14 is designed to operate on a variety of aircraft, including remotely piloted. It can locate and track the sun without input from an operator and record data in a self-contained data system. Using aircraft-provided data on latitude, longitude, and ambient static pressure, aerosol (or particulate) optical depth $\tau_p(\lambda)$ and CWV are computed in real time and displayed at the operator station (along with raw data, instrument status, and aircraft-provided data). Radiometric calibration is determined from Langley plots (Schmid and Wehrli 1995). Vertical differentiation of AOD and CWV data in suitable flight patterns yields extinction spectra and water vapor concentration. Examples of measurements in previous deployments are given by Russell et al. (1999), Schmid et al. (2000), Livingston et al. (2003), and Redemann et al. (2003).

Our methods for data reduction, calibration, and error analysis have been described previously (Russell et al. 1993; Schmid and Wehrli 1995; Schmid et al. 1998, 2001). A brief summary is given here. The AATS-14 channels are chosen to allow separation of aerosol, water vapor, and ozone transmission. From these slant-path transmissions we retrieve $\tau_p(\lambda)$ in 13 narrow wavelength bands and the columnar amounts of water vapor and ozone. In addition to corrections for Rayleigh scattering and O_3 absorption, some channels require corrections for NO_2, H_2O, and O_2–O_2 absorption. Cross sections were computed using Line-By-Line Radiative Transfer Model (LBLRTM) 6.01 (Clough and Iacono 1995) with the Clough–Kneizys–Davies (CKD) 2.4.1 continuum model using the high-resolution transmission molecular absorption database (HITRAN) 2000 (version 11.0) line list (Rothman et al. 2001; Rothman and Schroeder 2002) (including an update for water vapor from April 2001; see http://www.hitran.com/hitran/updates.html). NO_2 cross sections not included in LBLRTM 6.01 were taken from Harder et al. (1997). NO_2 was assumed constant at 2×10^{-15} molecules cm^{-2}, contributing about 0.003 to the optical depth at 0.449 μm. The CLAMS AATS-14 dataset consists of 13 wavelengths (0.354, 0.380, 0.449, 0.499, 0.525, 0.606, 0.675, 0.778, 0.865, 1.019, 1.059, 1.241, and 1.558 μm) at which we retrieve $\tau_p(\lambda)$ and the 0.94-μm wavelength, which we use to determine CWV (Schmid et al. 2001). AATS-14 was calibrated at the Mauna Loa Observatory (MLO), Hawaii, in June and September of 2001 using the Langley plot technique (Schmid and Wehrli 1995), effectively bracketing the CLAMS campaign. As a result of bandpass-filter degradation, the calibration constants obtained from the postmission calibration were lower than those obtained from the pre-mission calibration. However, for 7 of the 14 wavelengths the change was only 0.6% or less. Four of the remaining seven channels had degraded by less than 2%, and the remaining three channels (0.449, 0.606, and 0.940 μm) had degraded by 2.8% to 4%. Because we had no indication of an abrupt change in the calibration constants we used the average of the June and September calibration constants, effectively assuming that the calibration change happened gradually over time. We considered the change in calibration constants by including a statistical uncertainty in the calibration constants equal to half the range between pre- and postmission calibration.

Because sun photometers have a nonzero field of view (FOV), they measure some diffuse light in addition to the direct solar beam. As a result, uncorrected sun-photometer measurements can overestimate direct-beam transmission and hence underestimate $\tau_p(\lambda)$. This effect increases with decreasing wavelength and increasing particle size in the column. We estimated these diffuse light effects using formulations derived by Russell et al. (2004), which are applicable over a wide range of column particle size distributions containing large and small aerosol particles. However, because of the predominance of small particles in the CLAMS campaign, these diffuse light corrections were generally negligible.

After consideration of all possible sources of error, the AATS-14–derived AOD had the highest uncertainties for those channels with the largest difference in pre- and postmission calibration. For example, the uncertainties in AOD at 0.606 μm for the "golden" CLAMS flight on 17 July, spanning aerosol airmass factors from 1.1 to 1.9, yielded a mean value of ~0.013, with a maximum value of ~0.017.

b. Aerosol Robotic Network

The Aerosol Robotic Network (Holben et al. 1998) of ~200 identical globally distributed sun- and sky-

scanning ground-based automated radiometers provides measurements of aerosol optical properties, based on 10 yr of observations in some locations. These data have the potential to narrow the uncertainty in knowledge of the aerosol optical properties and are therefore used extensively in satellite sensor validation studies. The spectral sky radiance is measured in a wide angular range from the sun and is minimally affected by surface reflectance (cf. Dubovik and King 2000). AERONET imposes instrument, calibration, and processing standards that allow quantitative results to be intercomparable between all globally distributed sites throughout the decade-long record of observations (Holben et al. 1998; Holben et al. 2001; Smirnov et al. 2000). The ground-based measurements of aerosol optical depth carried out by AERONET have been invaluable in providing continuous statistically relevant aerosol observations in support of satellite sensor validations and aerosol characterization. In addition, the inversion of AERONET sky-radiance measurements to retrieve aerosol size and refractive index information has aided in the regional adjustments of MODIS aerosol retrieval algorithms (by providing regionally representative aerosol single scattering albedos) and in the general assessment of aerosol–climate interactions. An AERONET Cimel sun photometer has been permanently situated at the COVE platform (36.9°N, 75.71°W) since October 1999. In this study, we made use of the AERONET-derived AOD data for the assessment of mutual consistency with the airborne AATS-14 measurements.

c. MODIS retrievals of aerosol optical depth

The approach of the MODIS over-ocean algorithm for the retrieval of aerosol optical depth is similar to that of the land algorithm (Tanré et al. 1997), but the channels used and other features are quite different (Remer et al. 2005). In the first step, the reflectances from the six channels at 0.55, 0.66, 0.86, 1.24, 1.6, and 2.13 μm are grouped into nominal 10-km boxes of 20 $\times$ 20 pixels at 500-m resolution. The standard MOD35 cloud mask uses the brightness in the visible channels to identify clouds. This procedure will mistake heavy aerosol as cloudy and can miss important aerosol events over the ocean (Remer et al. 2005; Martins et al. 2002). On the other hand, relying solely on IR tests permits low-altitude, warm clouds to be misidentified as "clear," introducing cloud contamination in the aerosol products. Thus, the cloud mask used in the MODIS aerosol retrieval algorithm is based on the difference in spatial variability between aerosols and clouds. It computes the standard deviation of 0.55-μm reflectances in every group of 3 $\times$ 3 pixels within a box (Martins et al. 2002). Any group of nine contiguous pixels with standard deviation greater than 0.0025 is labeled as "cloudy," and all nine pixels in the group are discarded. This test separates aerosol from most cloud types, but may fail at the centers of large, thick clouds and with cirrus, both of which can be spatially homogeneous. It may also erroneously identify inhomogeneous aerosol fields (e.g., dust) as clouds. In an effort to avoid both scenarios, additional spectral dependence filters, which make use of the "flat" wavelength dependence of cloud optical depth, are applied.

Initial validation efforts of the MODIS level 2 aerosol data product (MOD04_L2) were carried out by Remer et al. (2002) for the over-ocean products based on 2 months of AERONET data in 2000, and by Chu et al. (2002) for the over-land AOD based on 3 months of AERONET data also in 2000. Since then, Levy et al. (2003) analyzed the performance of the over-ocean algorithm in the presence of dust, Levy et al. (2005) studied the performance of the land and ocean algorithm in the context of CLAMS, and Remer et al. (2005) presented a validation effort of both the land and ocean algorithms based on 2 yr of AERONET data. In the most comprehensive of these studies, Remer et al. (2005) found that one standard deviation of all MODIS AOD retrievals (when compared to AERONET AOD measurements) fall within the predicted uncertainty $\Delta\tau = \pm 0.03 \pm 0.05\tau$ over ocean and $\Delta\tau = \pm 0.05 \pm 0.15\tau$ over land. All these validation studies used the validation approach developed by Ichoku et al. (2002), which entails averaging the MODIS data over nominally 50 km $\times$ 50 km boxes and averaging the AERONET measurements over 1 h. In this paper, we investigate the implications of spatial averaging in the standard MODIS validation approach in the vicinity of the COVE platform, which is used as an AERONET site for MODIS validation work.

d. MISR retrievals of aerosol optical depth

MISR produces 36 simultaneous views of the earth, in a combination of nine angles varying from +70° to −70° in the along-track direction, in each of four spectral bands centered at 0.446, 0.558, 0.672, and 0.867 μm (Diner et al. 1998). It takes 7 min for all nine MISR cameras to view a fixed line on the surface, which sets the effective temporal resolution for coincident observations. At midlatitudes, all locations are imaged about once per week in global mode, providing 275-m resolution data in all four nadir channels, and in the red channels of the other eight cameras. The remaining 24 channels of data are averaged on board the spacecraft to 1.1-km resolution. For the five MISR event days during CLAMS (10, 17, 19, and 26 July and 2 August), the COVE platform was also designated as a MISR local-mode site, which means that over an area 300 km along track and 360 km cross track, MISR data were acquired at 275-m resolution in all 36 channels.

Prelaunch theoretical studies indicated that MISR spectral radiances, measured at precisely known airmass factors ranging from 1 to 3, could provide tight constraints on AOD over land and water. Along with

the wide range of scattering angles sampled (about 50°–160° at midlatitudes), MISR offers constraints on particle shape, size distribution, and composition, particularly over dark, uniform ocean surfaces (Kahn et al. 2001b; Martonchik et al. 1998).

The present study is one of several that involve field measurements to assess the sensitivity of aerosol retrievals based on satellite multiangle imaging (cf. Diner et al. 2001). In addition, the assumptions made in the retrieval algorithm about aerosol component particle properties, scene variability, and other factors must be critically tested and refined. Together with studies from the Aerosol Characterization Experiment-Asia (ACE-Asia) and Southern African Regional Science Initiative (SAFARI), the current study is part of an ongoing MISR validation effort aimed at defining a few satellite scenes very carefully and in detail to then extrapolate the findings regarding the performance of the aerosol retrieval algorithm. Since scene variability was determined in prelaunch studies to contribute significantly to the uncertainties in the aerosol retrievals, and since AOD variability is one of the main contributors to scene variability over the ocean, the analysis of spatial variability of AOD at and below the MISR retrieval grid performed in this paper should support the assessment of the performance of the MISR aerosol retrieval algorithm.

3. Results

a. Comparisons of AOD from AATS-14 and AERONET at COVE

During CLAMS, the CV-580 aircraft carrying AATS-14 flew in the vicinity of the heavily instrumented COVE platform site (36.9°N, 75.71°W) on 11 occasions. Among the instrumentation stationed at COVE were a micropulse lidar (MPL; Welton et al. 2001) as well as an AERONET Cimel sun photometer (Holben et al. 1998). The Cimel sun photometer was mounted 37 m above sea level. For one of the 11 CV-580 flybys, 26 July, AERONET was not able to measure AOD within 45 min of the flyby. The remaining 10 occasions are opportunities to compare the AATS-14–derived AOD spectra to the AERONET-derived AOD spectra. It should be noted that among the 7 AERONET wavelengths (0.34, 0.38, 0.44, 0.50, 0.67, 0.87, and 1.02 μm) and the 13 AATS-14 AOD wavelengths (0.354, 0.380, 0.449, 0.499, 0.525, 0.606, 0.675, 0.778, 0.865, 1.019, 1,059, 1.241, and 1.558 μm), 5 nearly exact AERONET/AATS-14 wavelength matchups at 0.38/0.38, 0.50/0.499, 0.67/0.675, 0.87/0.865 and 1.02/1.019 μm are provided. Figure 1 shows the comparisons of AERONET- and AATS-14-derived AOD at the shortest two and the longest two wavelength pairs, with the 0.67/0.675 pair not shown for brevity and lack of infor-

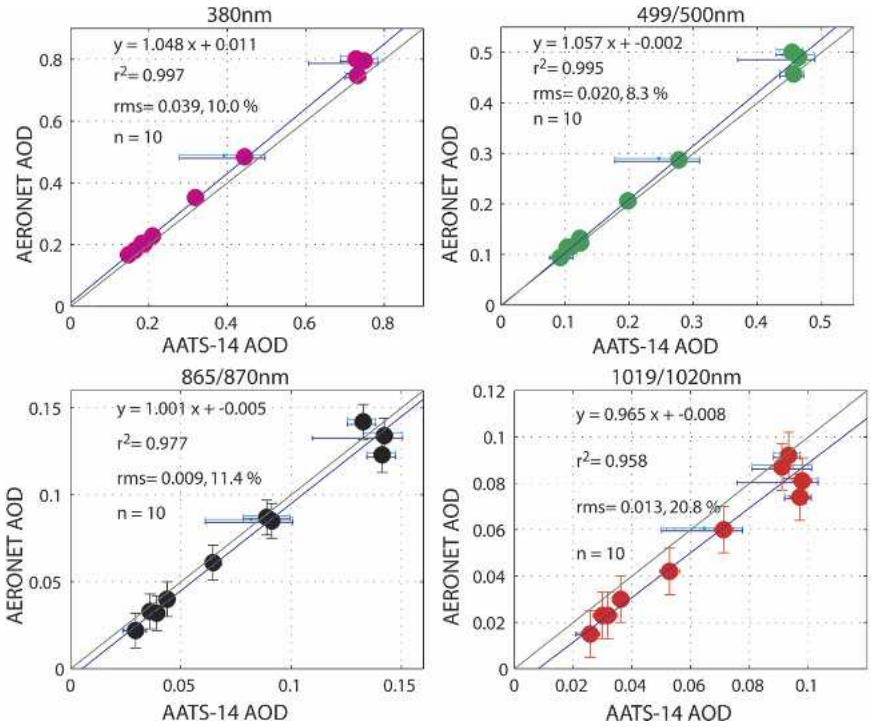

FIG. 1. Comparison of AOD derived from the AATS-14 and the AERONET Cimel sun photometer at the COVE platform (36.9°N, 75.71°W). Data are shown for four wavelengths. AATS-14 data were taken during low-level flight legs at a distance less than 6 km from COVE and at flight altitudes below 80 m. The light and dark blue error bars on the AATS-14 data represent the maximum variability within a range of 17 and 50 km from COVE, respectively.

mation different from the other four wavelength pairs. The AATS-14-derived AODs are taken as averages of short time spans (usually less than 90 s) when the CV-580 was closest to COVE, generally within 6 km and at flight altitudes below 80 m. It can be seen that AATS-14 and AERONET are generally well correlated with *r*-square values of 0.958 at 1.02 μm increasing to 0.997 at 0.38 μm. The rms differences at the three shortest wavelengths are of the order of 10% (relative rms difference calculated as the rms difference divided by the mean AOD), yet the rms difference at 1.02 μm is larger, at about 20.8%. The AATS-14 AODs at 1.02 μm are generally larger than the AERONET values by about 0.01, which is significant at this wavelength. Also shown in Fig. 1 are "error" bars on the AATS-14 AOD data that depict minimum and maximum values retrieved within a 10-km radius (light blue) and 50-km radius (dark blue) of the COVE site. From the occasional location of these error bars to the left of the actual data points, it can be seen that the AERONET COVE site was sometimes collocated with the maxima in the regional AOD fields.

To explore this phenomenon further, and to assess the adequacy of the COVE platform as a satellite validation site, Table 1 summarizes the spatial statistics of the AATS-14-derived AOD fields during nine low-level flight legs centered at or in the vicinity of COVE. Data are given for distances within 6, 17, and 50 km of COVE, respectively, and for wavelengths of 0.354, 0.499, 0.865, 1.019, and 1.558 μm. Two cases included in the AATS-14/AERONET comparisons in Fig. 1 are not shown in Table 1, since the flight legs for those comparisons were too short to study AOD variability on the spatial scales of interest. The case study for 26 July was added to Table 1, although there was no AERONET level 2 data to compare to AATS-14 in Fig. 1. For each case study, Table 1 summarizes the mean (μ_s) and the standard variation (σ_s) of the five-wavelength AOD data within the three distances (6, 17, and 50 km) of COVE. Also shown are the percentage differences of the mean AODs at the two scales from the mean AOD closest to COVE, namely,

$$\Delta\mu_s = \frac{|\mu_{s,<6\text{km}} - \mu_{s<x\text{km}}|}{\mu_{s,<6\text{km}}}, \quad (1)$$

where $\mu_{s,<6\text{km}}$ denotes the mean AOD in the closest possible proximity to the COVE site (generally < 6 km) and x is either 17 or 50 km. Six of the nine low-level flight tracks that went into Table 1 are shown in Fig. 2. From Table 1, it can be seen that in three cases (cases 2, 3, and 6) the mean AODs changed significantly when the data were averaged over larger areas. For cases 2 and 6, the differences in mean AOD in the closest vicinity to COVE as compared to a 50-km radius often exceeded 20%. There was no significant wavelength dependence in the AOD differences.

When we compare the AOD data in going from the closest proximity to COVE to the 17-km radius, the standard deviations increase in five out of nine cases and are constant in the remaining four. In going from the 17- to the 50-km data, only six cases show data for both spatial scales. Out of those six cases, the standard deviations increase for three cases, stay constant for two cases, and decrease for one case. Hence, in general, standard deviations of AATS-14 AOD data increase with increasing spatial scale up to 50 km.

Another way of looking at spatial variability is depicted in Figs. 2 and 3. Figure 2 shows all CV-580 low-level flight tracks that extended at least 20 km horizontally. In addition to seven low-level flight legs in the vicinity of COVE that satisfied this criterion, two more flight legs flown on 12 and 23 July are shown. Figure 3 shows both the absolute (left panels) and the relative (right panels) difference in AOD from the AOD at the starting point of the low-level flight leg as a function of the horizontal distance from that point. At the UV (0.354 μm) and the midvisible (0.499 μm) wavelength, the largest absolute gradients in AOD were 0.1–0.2 per 50-km horizontal distance. At 1.019 and 1.558 μm, analogous gradients rarely measured 0.05. Figure 3 also shows that the relative gradients in AOD were remarkably similar for all wavelengths, with maximum values of 70% per 50 km and more typical values of 25%.

To estimate an average relative change per horizontal distance, we performed least squares no-offset linear fits to the absolute values of AOD difference versus horizontal distance. The no-offset straight-line fits to the relative AOD differences show slopes between 0.47 and 0.64, although the straight-line fit is probably a poor approximation to the data, as indicated by the low correlation coefficients.

b. *Comparisons of AATS-14- and MODIS-derived over-ocean AOD*

AATS-14's participation in CLAMS was intended to support the over-ocean AOD validation of MODIS and MISR on *Terra*. An additional objective of the MODIS team was the development of an in-glint retrieval algorithm for AOD and aerosol column absorption. Consequently, the CV-580 aircraft carrying AATS-14 was frequently located in regions of MODIS glint during *Terra* overpass time. Therefore, only a few nonglint validation opportunities for the MODIS aerosol product (MOD04_L2) presented themselves. Here we summarize the MODIS/AATS-14 comparisons from three nonglint retrieval scenes on 14, 23, and 31 July. On 14 and 31 July, winds at the surface were generally northerly, while the wind was southerly on 23 July. AOD on all three days was moderate (see Figs. 5 and 6). Magi et al. (2005) found that on 23 July, there was less carbon fraction, higher RH, and larger sulfate fraction than on 14 and 31 July. The goal of this study is to perform true over-ocean validations (rather than over-ocean validation with ground-based, coastal sites) at finer spatial

TABLE 1. Comparison of AATS-14 AOD measurements for nine flight legs during CLAMS in the vicinity of COVE. Data are given for five wavelengths. For each wavelength the mean AOD is shown for three different spatial scales: 6 km—closest to COVE; 17 km—averaged over all data within a distance of 17 km from COVE; and 50 km—averaged over all data within a distance of 50 km from COVE. Standard deviations are given for all data within the respective spatial scales along with the relative differences of the mean AOD within the larger two scales compared to the mean AOD within the smallest scale [cf. Eq. (1)]. Relative differences larger than 5% are shown in bold.

		0.354 μm			0.499 μm			0.865 μm			1.019 μm			1.558 μm		
Case		6 km	17 km	50 km	6 km	17 km	50 km	6 km	17 km	50 km	6 km	17 km	50 km	6 km	17 km	50 km
1 Jul 10 1823 UTC	μ_s	0.344	0.353	n/a	0.198	0.203	n/a	0.065	0.066	n/a	0.053	0.054	n/a	0.041	0.041	n/a
	σ_s	0.001	0.009	n/a	0.001	0.005	n/a	0.000	0.002	n/a	0.000	0.001	n/a	0.001	0.001	n/a
	$\mu_{s,<6\text{km}}$ [%]	n/a	2.8	n/a	n/a	2.6	n/a	n/a	2.3	n/a	n/a	2.1	n/a	n/a	1.2	n/a
2 Jul 10 1858 UTC	μ_s	0.484	0.349	0.373	0.278	0.205	0.215	0.091	0.069	0.071	0.071	0.056	0.057	0.048	0.041	0.042
	σ_s	0.004	0.073	0.049	0.002	0.040	0.025	0.001	0.012	0.007	0.001	0.008	0.005	0.000	0.004	0.002
	$\mu_{s,<6\text{km}}$ [%]	n/a	**27.9**	**22.9**	n/a	**26.3**	**22.6**	n/a	**24.0**	**22.5**	n/a	**21.6**	**20.1**	n/a	**14.9**	**14.1**
3 Jul 14 1534 UTC	μ_s	0.193	0.185	0.184	0.093	0.089	0.088	0.030	0.028	0.028	0.026	0.025	0.024	0.021	0.020	0.020
	σ_s	0.011	0.016	0.015	0.005	0.008	0.008	0.001	0.002	0.002	0.001	0.002	0.002	0.001	0.002	0.002
	$\mu_{s,<6\text{km}}$ [%]	n/a	4.0	4.4	n/a	4.4	4.9	n/a	**5.1**	**5.8**	n/a	4.7	**5.8**	n/a	**5.1**	**6.5**
4 Jul 17 1612 UTC	μ_s	0.859	0.846	0.824	0.464	0.457	0.444	0.142	0.140	0.136	0.098	0.097	0.094	0.050	0.049	0.048
	σ_s	0.016	0.019	0.041	0.012	0.012	0.026	0.004	0.004	0.008	0.003	0.003	0.006	0.001	0.001	0.003
	$\mu_{s,<6\text{km}}$ [%]	n/a	1.5	4.1	n/a	1.6	4.4	n/a	1.4	4.3	n/a	1.4	4.5	n/a	1.6	4.8
5 Jul 17 1632 UTC	μ_s	0.839	0.828	n/a	0.456	0.449	n/a	0.141	0.139	n/a	0.097	0.095	n/a	0.050	0.049	n/a
	σ_s	0.014	0.014	n/a	0.009	0.009	n/a	0.003	0.003	n/a	0.002	0.002	n/a	0.001	0.001	n/a
	$\mu_{s,<6\text{km}}$ [%]	n/a	1.3	n/a	n/a	1.6	n/a	n/a	1.6	n/a	n/a	2.0	n/a	n/a	2.0	n/a
6 Jul 26 1555 UTC	μ_s	0.555	0.552	0.400	0.437	0.451	0.316	0.201	0.218	0.154	0.152	0.165	0.119	0.074	0.079	0.068
	σ_s	0.032	0.033	0.112	0.030	0.032	0.100	0.023	0.020	0.049	0.021	0.017	0.036	0.016	0.009	0.013
	$\mu_{s,<6\text{km}}$ [%]	n/a	0.6	**28.0**	n/a	3.3	**27.7**	n/a	**8.3**	**23.5**	n/a	**8.6**	**21.5**	n/a	**7.3**	**7.9**
7 Aug 2 1606 UTC	μ_s	0.197	0.200	0.205	0.103	0.105	0.108	0.036	0.037	0.037	0.030	0.030	0.031	0.021	0.022	0.022
	σ_s	0.004	0.010	0.013	0.002	0.005	0.007	0.001	0.001	0.002	0.000	0.001	0.001	0.000	0.001	0.001
	$\mu_{s,<6\text{km}}$ [%]	n/a	1.7	4.4	n/a	1.7	4.4	n/a	1.4	3.0	n/a	1.0	2.3	n/a	1.4	2.8
8 Aug 2 1622 UTC	μ_s	0.204	0.206	0.209	0.109	0.110	0.111	0.039	0.039	0.039	0.032	0.032	0.032	0.024	0.024	0.024
	σ_s	0.006	0.011	0.012	0.003	0.006	0.006	0.001	0.001	0.001	0.001	0.001	0.001	0.000	0.001	0.001
	$\mu_{s,<6\text{km}}$ [%]	n/a	1.2	2.5	n/a	1.0	2.0	n/a	0.5	0.5	n/a	0.0	0.0	n/a	0.0	0.4
9 Aug 2 1933 UTC	μ_s	0.228	0.226	n/a	0.123	0.122	n/a	0.044	0.043	n/a	0.036	0.036	n/a	0.029	0.029	n/a
	σ_s	0.006	0.005	n/a	0.003	0.003	n/a	0.001	0.001	n/a	0.001	0.001	n/a	0.001	0.001	n/a
	$\mu_{s,<6\text{km}}$ [%]	n/a	1.0	n/a	n/a	1.2	n/a	n/a	1.6	n/a	n/a	1.9	n/a	n/a	1.7	n/a

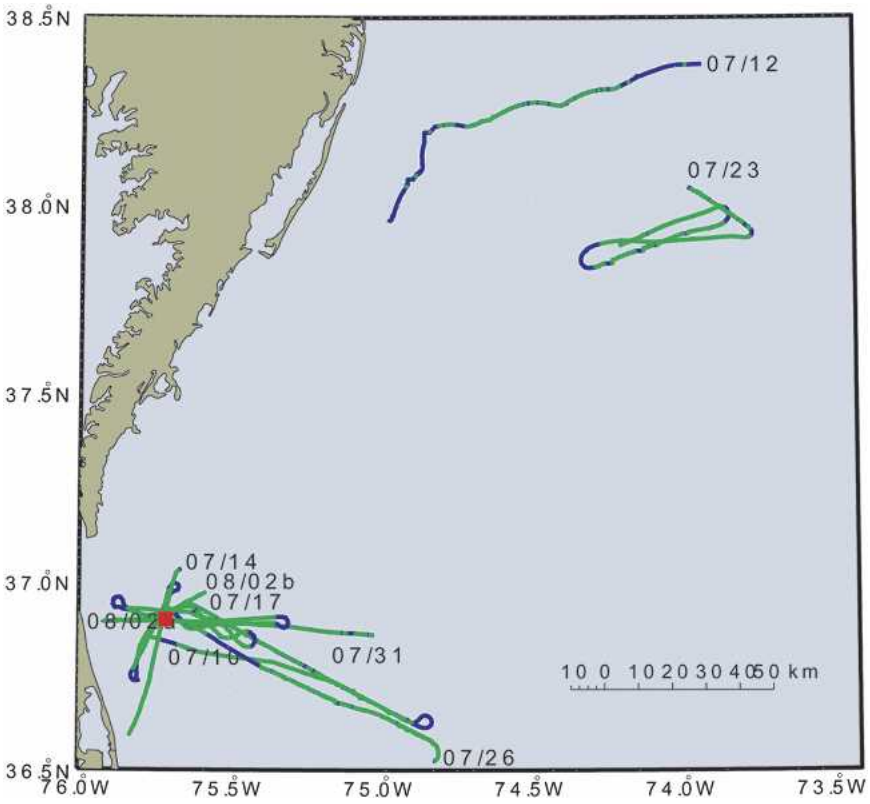

FIG. 2. Location of nine low-level flight legs of the University of Washington's CV-580 research aircraft in CLAMS. Green points mark locations of successful AATS-14 retrievals of AOD at flight altitudes below 80 m. Blue points indicate cloud contamination or a flight altitude above 80 m. The red square marks the location of the Chesapeake Lighthouse.

scales and extending to longer wavelengths than those considered in previous studies.

Figure 4 shows the location of the CV-580 flight tracks relative to the MODIS level 2 data grids, which have a nominal grid size of 10 km × 10 km in the nadir and stretch out toward the edges of the MODIS granules. As in Fig. 2, data points in blue along the flight tracks indicate an AATS-14 measurement, while the data points in green indicate a successful AATS-14 AOD retrieval at an aircraft altitude below 80 m. Only one of the three cases (14 July) was located in the vicinity of COVE; the other two cases were located over darker ocean water.

The three separate days provided a total of 16 exact matchups between AATS-14 and MOD04_L2, with AATS-14 measurements performed generally within 15 min of the *Terra* overpass time (see Fig. 5). Out of the 16 matchups, five took place on 14 July (Figs. 5a–e), seven on 23 July (Figs. 5f–l), and four on 31 July (Figs. 5m–p). It is noteworthy that the AOD for all 16 cases was ≤ 0.1 at a wavelength of 0.5 μm. Figures 5a–e also show the AERONET retrieval of AOD, averaged over the two AERONET level 2 retrievals at 1538 and 1553 UTC (*Terra* overpass at 1541 UTC). It can be seen that the curvature of the MODIS and AATS-14 spectra are very similar and that all data agree within the error bars. Starting at a wavelength of 0.87 μm, however, the AERONET AOD values are below the AATS-14–derived values, and MODIS values do not agree with AERONET values within the error bars. For the seven cases on 23 July (Figs. 5f–l), the MODIS-derived AOD values are generally below the AATS-14-derived values, but the two datasets again agree well within the error bars, even though the magnitude of AOD at 0.5 μm was only about 0.05. The four cases on 31 July exhibit the poorest agreement out of all three days. AATS-14-derived AOD for that day is only about half the MODIS-derived AOD at all wavelengths.

By fitting a quadratic function to AATS-14-derived ln(AOD) versus ln(λ), we can extrapolate the data beyond the longest AATS-14 wavelength (1.558 μm) to compare AATS data with the data at the longest MODIS wavelength of 2.14 μm. Using these quadratics for each case in Fig. 5 also enables us to calculate AATS-14 AOD values at the exact seven MODIS wavelengths (0.47, 0.55, 0.66, 0.87, 1.24, 1.64, and 2.14 μm). For the 16 matchups shown in Fig. 5 this process yields 112 data pairs of MODIS and AATS-14 AOD. These data pairs are plotted in Fig. 6, along with a least

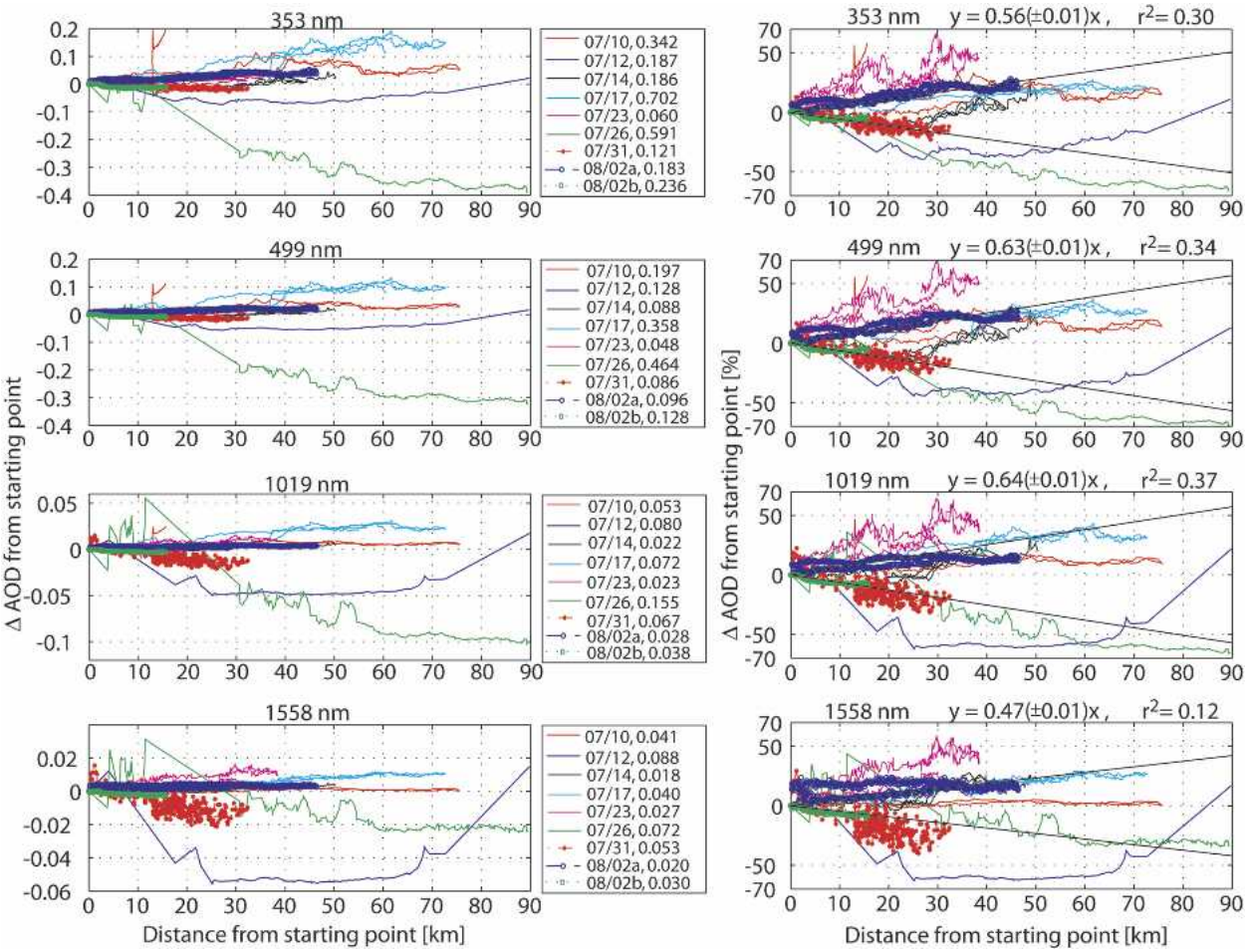

FIG. 3. Spatial variability in AODs derived from AATS-14 during the nine low-level flight legs shown in Fig. 2. Data are shown as (left) absolute differences and (right) relative differences from the AOD at the starting point of the low-level legs for four wavelengths (0.354, 0.499, 1.019, and 1.558 μm). The text in the legends gives the flight date and the starting point AOD for the respective legs.

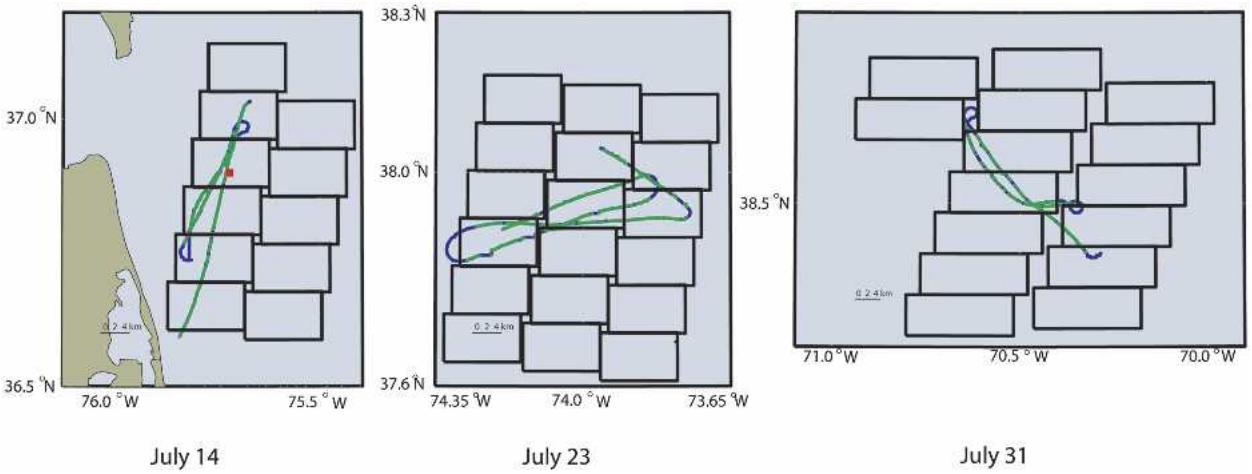

FIG. 4. CV-580 flight tracks relative to the location of MOD02_L2 aerosol retrieval boxes on 14, 23, and 31 Jul. See Fig. 2 for explanation of color code on the AATS-14 data points along the flight tracks.

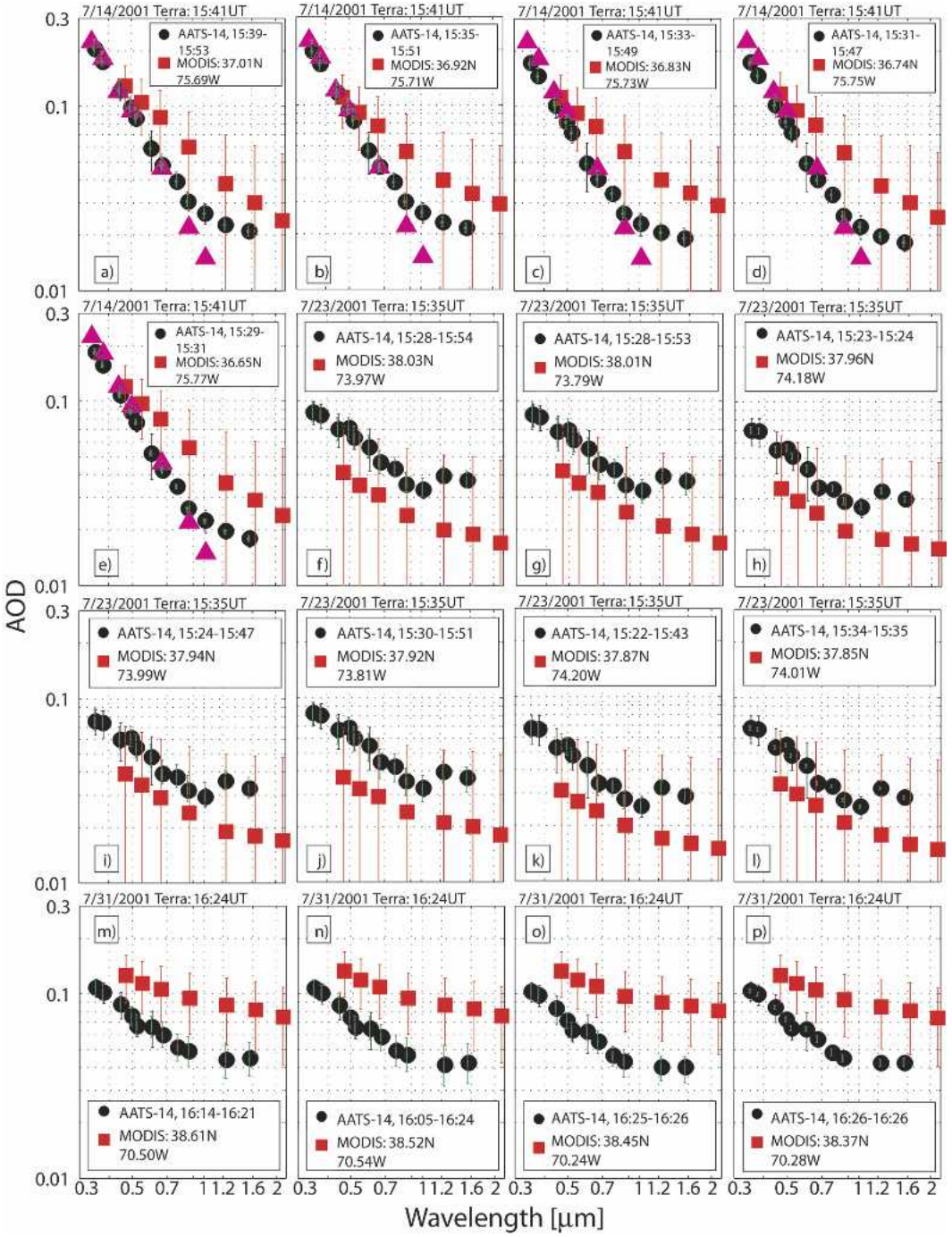

FIG. 5. Comparison of spectral AODs derived from AATS-14 and MOD04_L2 for the 16 collocated measurements shown in Fig. 4. Out of the 16 matchups, (a)–(e) five took place on 4 Jul, (f)–(l) seven on 23 Jul, and (m)–(p) four on 31 Jul. Also shown (as magenta triangles) are the AERONET AOD measurements at COVE closest in time to the *Terra* overpass time (as given in the title of each panel).

squares linear fit to the data and the MODIS prelaunch estimate of the over-ocean AOD error given by $\Delta\tau = \pm 0.03 \pm 0.05\tau$. It can be seen that while the fit and the correlation are relatively poor, only ~27% of all MODIS data points fall outside of the prelaunch error range. For comparison, Fig. 6 also shows the results of the regular MODIS validation approach as colored squares, reproduced from Levy et al. (2005). As explained above, in this approach all available MODIS data in nominally 5×5 10-km^2 boxes are averaged and

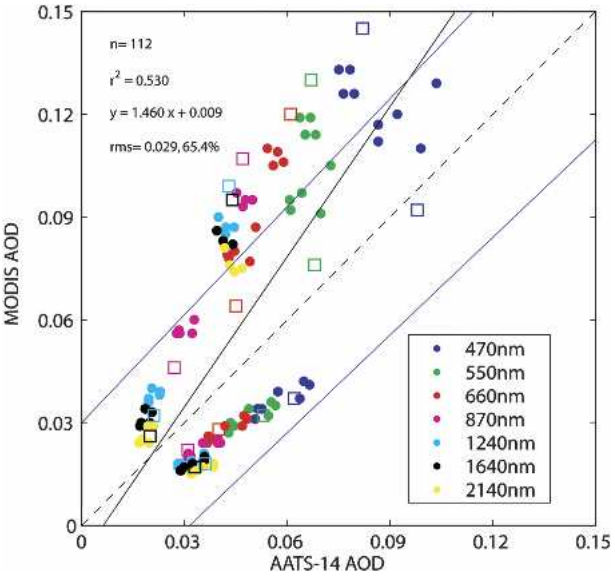

FIG. 6. Scatterplot of AOD derived from AATS-14 and MODIS for seven wavelengths and the 16 matchups given in Fig. 5. The 1:1 line is shown as a dashed line, while the solid black line represents the linear least squares fit to the data. The blue solid lines show the prelaunch estimated AOD uncertainty given by $\Delta\tau = \pm 0.03 \pm 0.05\tau$. Also shown as squares are the results of the standard MODIS validation approach (Levy et al. 2005), which averages the MODIS data in nominally 50 km × 50 km boxes centered on a validation site.

compared to the suborbital measurements within a certain time period around satellite overpass time, here ±20 min. Effectively, this approach compares the suborbital measurements to MODIS data averaged over a larger spatial domain, yielding only one comparison between MODIS and AATS-14 per day. In Fig. 6, this approach results in data pairs that are closer to the 1:1 line for one of the study days, farther away from the 1:1 line for another day and seemingly an unchanged situation for the third day (i.e., the day with the lowest MODIS-derived AOD).

c. *Comparisons of AATS-14- and MISR-derived over-ocean AOD*

On four days during CLAMS, MISR aboard *Terra* sampled the region around the COVE site in local mode, effectively increasing the spatial resolution of all 36 channels to 275 m. These days were 10, 17, and 26 July and 2 August. In addition, AirMISR flew aboard the NASA ER-2 aircraft and collected data in the vicinity of COVE on 12 and 31 July. In this paper, however, we only present data from the standard MISR AOD algorithm, which retrieves AOD at a scale of 16 × 16 pixels (1.1 km each), resulting in a retrieval box of 17 km × 17 km. On 10 July, the CV-580 aircraft was not cleared to take off until after the *Terra* overpass time, and hence did not collect collocated data with MISR. Figure 7 shows the location of the CV-580 flight tracks on the other three days and the boxes for which the standard MISR AOD retrieval algorithm reported successful AOD retrievals. For the data on 26 July, the MISR algorithm screened out all data collocated with the CV-580 flight track (likely because of cloud contamination), reducing the number of days with useful comparisons to two. The gaps in the lower row of pixels on 17 July and 2 August are caused by the algorithm identifying those areas as shallow water (case 2).

Figure 8 shows the comparison of spectral AOD data from AATS-14 and MISR for seven pixels, five on 17 July and two on 2 August. According to Magi et al. (2005), 45%, 29%, 23%, and 3% of the total aerosol optical depth on 17 July were caused by sulfate, water, carbonaceous, and absorbing aerosols, respectively. On 2 August, the roles of sulfates and carbon were effectively reversed. MISR data are given at 0.446, 0.558, 0.672, and 0.867 μm. Also shown are the AERONET retrievals at COVE at 1617 UTC on 17 July and at 1609 UTC on 2 August. It should be noted, however, that Fig. 8a represents the best spatial collocation of AATS-14 and MISR data with AERONET on 17 July, and Fig. 8f represents the best collocation on 2 August. The AOD on 17 July was among the highest measured dur-

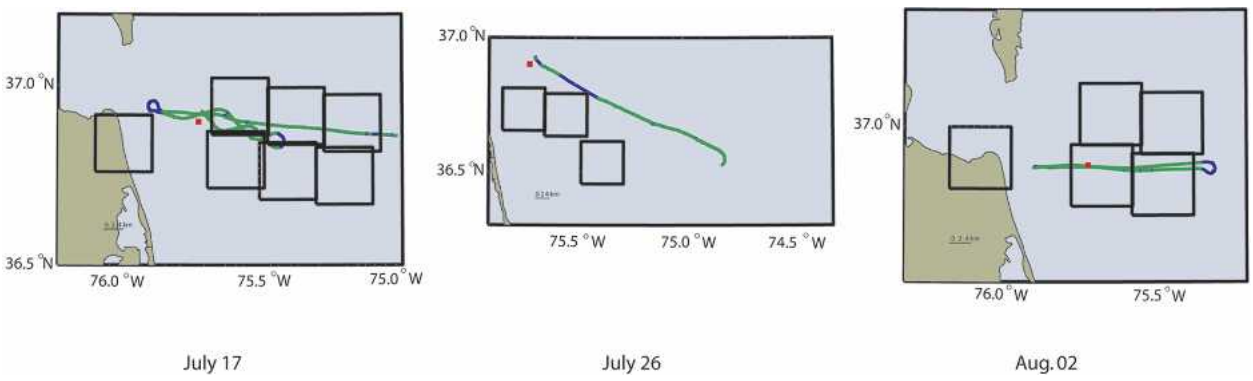

FIG. 7. CV-580 flight tracks relative to the location of the successful MISR standard retrieval algorithm boxes on 17 and 26 Jul and 2 Aug. See Fig. 2 for explanation of color code on the AATS-14 data points along the flight tracks.

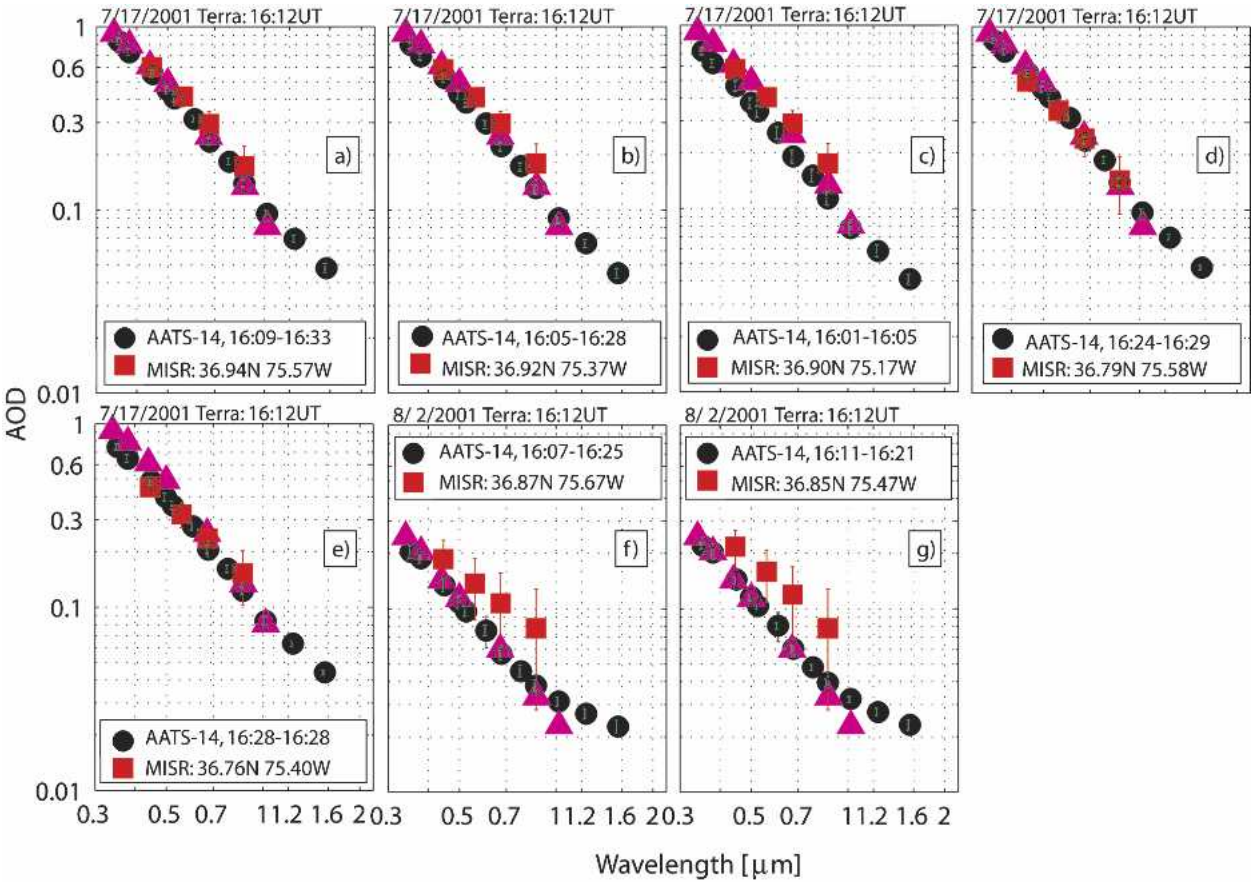

FIG. 8. Comparison of spectral AODs derived from AATS-14 and the MISR standard algorithm (regional mean) for the seven collocated measurements shown in Fig. 7. Out of the seven matchups, (a)–(e) five took place on 17 Jul and (f)–(g) two on 2 Aug. Also shown (as magenta triangles) are the AERONET AOD measurements at COVE closest in time to the *Terra* overpass time (as given in the title of each panel).

ing CLAMS, with values around 0.4–0.5 at 0.5 μm. Figure 9 shows the scatterplot of MISR- versus AATS-14-derived AOD for all four MISR wavelengths and all seven retrieval boxes shown in Fig. 8. The data show a strong correlation, with an r square of 0.94, but with an rms difference of 0.06 (26%). The least squares linear fit yields a slope of 0.97 and an offset of 0.054. Most or all of this discrepancy is traced to the MISR low-light-level calibration (Kahn et al. 2005). A MISR radiance scale correction, of order 5%, is expected, based on detailed analysis of vicarious calibration and laboratory data (Bruegge et al. 2004; Kahn et al. 2004, manuscript submitted to *J. Geophys. Res.*).

4. Conclusions

We carried out studies of the spatial variability of aerosol optical depth (AOD) off the U.S. central East Coast in July and August of 2001. Based on measurements in the vicinity of the CERES Ocean Validation Experiment (COVE) platform (36.9°N, 75.71°W), the spatial variability in AOD on scales of up to 100 km was assessed. During 10 flybys of the University of Washington CV-580 aircraft at the COVE site, comparisons of AATS-14 and an AERONET Cimel sun photometer located at COVE showed good agreement and high correlation coefficients (0.98 and higher) for wavelengths between 0.38 and 0.87 μm. At 1.02 μm, AATS-14 measured systematically higher AOD by about 0.01. The rms differences of greater than 20% between the two datasets at 1.02 μm suggest the inappropriate treatment of gaseous absorption in either retrieval algorithm or the possible poor calibration of the 1.02-μm channel in one of the two instruments. The AATS-14 measurements used in these comparisons were generally obtained in the immediate vicinity of the COVE-AERONET site, only allowing data that were measured within a distance of 6 km. Since the MODIS validation procedure is to average the AOD data from 5×5 pixels (nominally 50 km $\times$ 50 km at nadir) centered at a given validation site we also sought to characterize the spatial variability in AOD on those scales. For that purpose we compared spatially averaged mean AOD in the closest proximity of COVE and within 17-

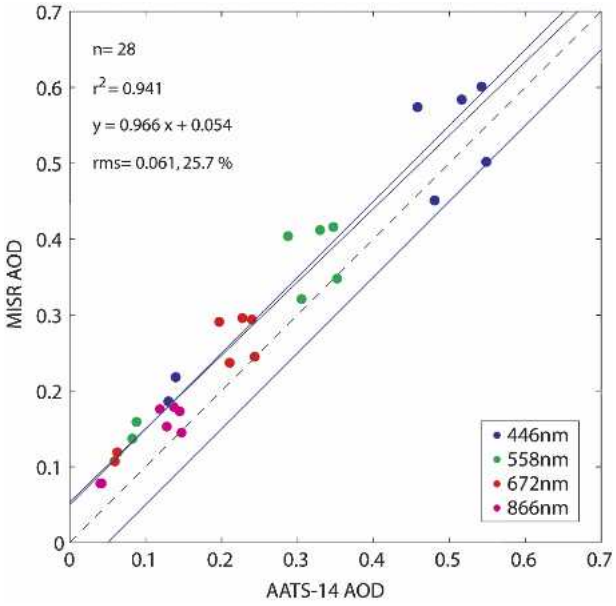

FIG. 9. Scatterplot of AATS-14 and regional mean MISR AOD (standard algorithm) for the four MISR wavelengths and the seven matchups given in Fig. 8. The 1:1 line is shown as a dashed line, while the solid black line represents the linear least squares fit to the data. The blue solid lines show the generic preliminary AOD uncertainty of 0.05.

and 50-km distances, respectively. In three out of nine cases, the mean AODs within both the 17- and the 50-km radius were significantly different from the mean AOD at the closest proximity. This finding differs from previous findings of the spatial pattern of AOD based on MODIS data (Ichoku et al. 2002), and it raises the question whether spatial variability contributed to the remaining differences in previous comparison studies between MODIS and suborbital measurements of spectral AOD.

An analysis of the spatial variability of AOD data, including two flight legs not in the vicinity of COVE, showed that AOD can vary by as much as 50%–70%, but more typically 25%–30% over horizontal distances of 50 km. Note that this variability does not address the differences in spatial mean AODs, but rather only the possible maximum variations between quasi-instantaneous AOD measurements. Note also that we found no spectral dependence of the relative variability in AOD. This suggests that the spatial variability in AOD off the U.S. East Coast is caused by the transport and diffusion of similar aerosol types rather than the mixing of aerosol types of different size and composition.

The comparisons of AATS-14- and MODIS-derived level 2 AOD data products in this study are different from previous AOD validation studies in that we (i) use single level 2 MODIS data boxes (10 km $\times$ 10 km at nadir), (ii) use suborbital data extending to a wavelength of 1.558 μm to extrapolate to the longest MODIS wavelength at 2.14 μm, and (iii) perform validation over dark water by using airborne sun-photometer measurements. Because of different objectives for AATS-14 in CLAMS, only a limited number of these validation opportunities occurred, all of which took place with very small aerosol loadings and consequently low AODs of 0.1 or below in the midvisible. The curvature of the MODIS-derived AOD spectra compared well with the shape of the AATS-14-derived AOD spectra, although there was a systematic difference between the two AOD datasets on any given day. Overall, the MODIS–AATS-14 comparisons showed relatively weak correlations and rms differences of 0.03 (65%). Nonetheless, 73% of all MODIS data points were within the prelaunch predicted error range of 0.03 $\pm$ 0.05 AOD. The systematic nature of the differences may be due to the limited choice of aerosol models for the MODIS retrievals or possibly due to the assumptions regarding sea surface conditions. In the MODIS aerosol retrievals, the specular reflection on the sea surface is calculated using a rough ocean model from Cox and Munk (1954), with the percentage of the sea covered by foam depending on the wind speed according to Koepke (1984). However, the wind speed is assumed to be spatially and temporally constant at 6 m s^{-1}. For 31 July, the study day with the largest discrepancy between AATS-14- and MODIS-derived AOD presented here, the Cloud Absorption Radiometer (CAR) measurements aboard the University of Washington Convair CV-580 (Gatebe et al. 2005) aircraft were inverted to yield wind speeds in excess of 10 m s^{-1}, while the nearby buoy measurements yielded a value of 8.4 m s^{-1}. The deviation of the true wind speed from the MODIS-assumed value of 6 m s^{-1} may be the main reason for the poor agreement between the AATS-14- and MODIS-derived AOD data for that day.

The comparisons of AATS-14 and coincident standard MISR aerosol products for CLAMS show strong correlation. The MISR values are systematically offset by 0.05–0.06 toward larger AOD at all wavelengths, consistent with MISR–AATS comparison results from ACE-Asia and SAFARI-2000. Since the release of the MISR aerosol product used in this study, most or all of this discrepancy has been traced to the MISR low-light-level calibration (Kahn et al. 2005). Because of the systematic nature of the difference, coupled with the high correlation, we expect that the application of the newly developed calibration to the MISR radiances collected in CLAMS will bring the two sets of AOD measurements into very tight agreement. The MISR results used in this study indicate that a lack of small, spherical nonabsorbing particles in an earlier version of the MISR standard aerosol retrieval algorithm, which made the spectral slope of the MISR results too shallow (Schmid et al. 2003), has been corrected. Further comparisons between AATS-14 data collected in CLAMS and the higher-resolution (275 m) MISR data are planned.

Acknowledgments. This research was supported by grants through the NASA New Investigator Program (NIP) in Earth Science, the NASA's Earth Observing System Inter-Disciplinary Science (EOS-IDS) Program, and NASA's Radiation Sciences Program (RSP). The participation of AATS-14 in CLAMS was made possible by a grant through the NASA EOS validation program. We thank Ms. S. Ramirez for help in producing the manuscript and figures.

REFERENCES

Bruegge, C. J., W. Abdou, D. J. Diner, B. J. Gaitley, M. Helmlinger, R. A. Kahn, and J. V. Martonchik, 2004: Validating the MISR radiometric scale for the ocean aerosol science communities. *Proceedings of the International Workshop on Radiometric and Geometric Calibration,* A. A. Balkema.

Chu, D. A., Y. J. Kaufman, C. Ichoku, L. A. Remer, D. Tanré, and B. N. Holben, 2002: Validation of MODIS aerosol optical depth retrieval over land. *Geophys. Res. Lett.,* **29,** 8007, doi:10.1029/2001GL013205.

Clough, S. A., and M. J. Iacono, 1995: Line-by-line calculations of atmospheric fluxes and cooling rates. II: Application to carbon dioxide, ozone, methane, nitrous oxide, and the halocarbons. *J. Geophys. Res.,* **100,** 16 519–16 535.

Cox, C., and W. Munk, 1954: Statistics of the sea surface derived from sun glitter. *J. Mar. Res.,* **13,** 198–208.

Diner, D. J., and Coauthors, 1998: Multiangle Imaging Spectroradiometer (MISR) description and experiment overview. *IEEE Trans. Geosci. Remote Sens.,* **36,** 1072–1087.

——, and Coauthors, 2001: MISR aerosol retrievals over southern Africa during the SAFARI-2000 dry season campaign. *Geophys. Res. Lett.,* **28,** 3127–3130.

Dubovik, O., and M. D. King, 2000: A flexible inversion algorithm for retrieval of aerosol optical properties from sun and sky radiance measurements. *J. Geophys. Res.,* **105,** 20 673–20 696.

Gatebe, C. K., M. D. King, A. I. Lyapustin, G. T. Arnold, and J. Redemann, 2005: Airborne spectral measurements of ocean directional reflectance. *J. Atmos. Sci.,* **62,** 1072–1092.

Harder, J. W., J. W. Brault, P. V. Johnston, and G. H. Mount, 1997: Temperature dependent NO_2 cross sections at high spectral resolution. *J. Geophys. Res.,* **102,** 3861–3879.

Holben, B. N., and Coauthors, 1998: AERONET—A federated instrument network and data archive for aerosol characterization. *Remote. Sens. Environ.,* **66,** 1–16.

——, and Coauthors, 2001: An emerging ground-based aerosol climatology: Aerosol optical depth from AERONET. *J. Geophys. Res.,* **106,** 12 067–12 097.

Ichoku, C., D. A. Chu, S. Mattoo, Y. J. Kaufman, L. A. Remer, D. Tanré, I. Slutsker, and B. Holben, 2002: A spatio-temporal approach for global validation and analysis of MODIS aerosol products. *Geophys. Res. Lett.,* **29,** 8006, doi:10.1029/2001GL013206.

Kahn, R., P. Banerjee, D. McDonald, and J. Martonchik, 2001a: Aerosol properties derived from aircraft multi-angle imaging over Monterey Bay. *J. Geophys. Res.,* **106,** 11 977–11 995.

——, ——, and ——, 2001b: Sensitivity of multiangle imaging to natural mixtures of aerosols over ocean. *J. Geophys. Res.,* **106,** 18 219–18 238.

——, B. J. Gaitley, J. V. Martonchik, D. J. Diner, K. A. Crean, J. V. Martonchik, and B. Holben, 2005: MISR global aerosol optical depth validation based on two years of coincident AERONET observations. *J. Geophys. Res.,* in press.

Kaufman, Y. J., D. Tanré, L. A. Remer, E. Vermote, A. Chu, and B. N. Holben, 1997: Operational remote sensing of tropospheric aerosol over land from EOS moderate resolution imaging spectroradiometer. *J. Geophys. Res.,* **102,** 17 051–17 067.

——, ——, and O. Boucher, 2002: A satellite view of aerosols in the climate system. *Nature,* **419,** 215–223.

Klett, J. D., 1985: Lidar inversion with variable backscatter/extinction ratios. *Appl. Opt.,* **24,** 1638–1643.

Koepke, P., 1984: Effective reflectance of oceanic whitecaps. *Appl. Opt.,* **23,** 1816–1823.

Levy, R. C., and Coauthors, 2003: Evaluation of the Moderate-Resolution Imaging Spectroradiometer (MODIS) retrievals of dust aerosol over the ocean during PRIDE. *J. Geophys. Res.,* **108,** 8594, doi:10.1029/2002JD002460.

——, L. A. Remer, J. V. Martins, Y. J. Kaufman, A. Plana-Fattori, J. Redemann, and B. Wenny, 2005: Evaluation of the MODIS aerosol retrievals over ocean and land during CLAMS. *J. Atmos. Sci.,* **62,** 974–992.

Livingston, J. M., and Coauthors, 2003: Airborne sun photometer measurements of aerosol optical depth and columnar water vapor during the Puerto Rico Dust Experiment and comparison with land, aircraft, and satellite measurements. *J. Geophys. Res.,* **108,** 8588, doi:10.1029/2002JD002520.

Magi, B., P. V. Hobbs, T. W. Kirchstetter, I. T. Novakov, D. A. Hegg, S. Gao, J. Redemann, and B. Schmid, 2005: Aerosol properties and chemical apportionment of aerosol optical depth at locations off the United States East Coast in July and August. *J. Atmos. Sci.,* **62,** 919–933.

Martins, J. V., D. Tanré, L. Remer, Y. Kaufman, S. Mattoo, and R. Levy, 2002: MODIS cloud screening for remote sensing of aerosols over oceans using spatial variability. *Geophys. Res. Lett.,* **29,** 8009, doi:10.1029/2001GL013252.

Martonchik, J. V., D. J. Diner, R. Kahn, M. M. Verstraete, B. Pinty, H. R. Gordon, and T. P. Ackerman, 1998: Techniques for the retrieval of aerosol properties over land and ocean using multiangle imaging. *IEEE Trans. Geosci. Remote Sens.,* **36,** 1212–1227.

Matsumoto, T., P. B. Russell, C. Mina, W. Van Ark, and V. Banta, 1987: Airborne Tracking Sunphotometer. *J. Atmos. Oceanic Technol.,* **4,** 336–339.

Ramanathan, V., P. J. Crutzen, J. T. Kiehl, and D. Rosenfeld, 2001: Aerosol, climate and the hydrological cycle. *Science,* **294,** 2119–2124.

Redemann, J., S. J. Masonis, B. Schmid, T. L. Anderson, P. B. Russell, J. M. Livingston, O. Dubovik, and A. D. Clarke, 2003: Clear-column closure studies of aerosols and water vapor aboard the NCAR C-130 during ACE-Asia, 2001. *J. Geophys. Res.,* **108,** 8655, doi:10.1029/2003JD003442.

Remer, L. A., and Coauthors, 2002: Validation of MODIS aerosol retrieval over ocean. *Geophys. Res. Lett.,* **29,** 8008, doi:10.1029/2001GL013204.

——, and Coauthors, 2005: The MODIS aerosol algorithm, products, and validation. *J. Atmos. Sci.,* **62,** 947–973.

Rothman, L. S., and J. Schroeder, 2002: Millenium HITRAN compilation. *Proc. 12th ARM Science Team Meeting,* St. Petersburg, FL, Dept. of Energy.

——, K. Chance, J. Schroeder, and A. Goldman, 2001: New edition of HITRAN database. *Proc. 11th ARM Science Team Meeting,* Atlanta, GA, Dept. of Energy.

Russell, P. B., and Coauthors, 1993: Pinatubo and pre-Pinatubo optical-depth spectra: Mauna Loa measurements, comparisons, inferred particle size distributions, radiative effects, and relationship to lidar data. *J. Geophys. Res.,* **98,** 22 969–22 985.

——, J. M. Livingston, P. Hignett, S. Kinne, J. Wong, and P. V. Hobbs, 1999: Aerosol-induced radiative flux changes off the United States Mid-Atlantic coast: Comparison of values calculated from sunphotometer and in situ data with those measured by airborne pyranometer. *J. Geophys. Res.,* **104,** 2289–2307.

——, and Coauthors, 2004: Sunlight transmission through desert dust and marine aerosols: Diffuse light corrections to Sun photometry and pyrheliometry. *J. Geophys. Res.,* **109,** D08207, doi:10.1029/2003JD004292.

Schmid, B., and C. Wehrli, 1995: Comparison of sun photometer calibration by Langley technique and standard lamp. *Appl. Opt.,* **34,** 4500–4512.

——, P. R. Spyak, S. F. Biggar, C. Wehrli, J. Sekler, T. Ingold, C. Mätzler, and N. Kämpfer, 1998: Evaluation of the applicability of solar and lamp radiometric calibrations of a precision sun photometer operating between 300 and 1025 nm. *Appl. Opt.,* **37,** 3923–3941.

——, and Coauthors, 2000: Clear sky closure studies of lower tropospheric aerosol and water vapor during ACE-2 using airborne sunphotometer, airborne in-situ, space-borne, and ground-based measurements. *Tellus,* **52B,** 568–593.

——, and Coauthors, 2001: Comparison of columnar water-vapor measurements from solar transmittance methods. *Appl. Opt.,* **40,** 1886–1896.

——, and Coauthors, 2003: Coordinated airborne, spaceborne, and ground-based measurements of massive thick aerosol layers during the dry season in southern Africa. *J. Geophys. Res.,* **108,** 8496, doi:10.1029/2002JD002297.

Smirnov, A., B. N. Holben, T. F. Eck, O. Dubovik, and I. Slutsker, 2000: Cloud screening and quality control algorithms for the AERONET data base. *Remote Sens. Environ.,* **73,** 337–349.

Smith, W., Jr., T. P. Charlock, R. Kahn, J. V. Martins, P. V. Hobbs, and L. A. Remer, 2005: EOS-Terra aerosol and radiative flux validation: An overview of the Chesapeake Lighthouse and Aircraft Measurements for Satellites experiment. *J. Atmos. Sci.,* **62,** 903–918.

Tanré, D., Y. J. Kaufman, M. Herman, and S. Mattoo, 1997: Remote sensing of aerosol properties over oceans using the MODIS/EOS spectral radiances. *J. Geophys. Res.,* **102** (D14), 16 971–16 988.

Welton, E. J., J. R. Campbell, J. D. Spinhirne, and V. S. Scott, 2001: Global monitoring of clouds and aerosols using a network of micro-pulse lidar systems. *Proc. SPIE,* **4153,** 151–158.